ACS Catalysis

Research Article

Cite This: ACS Catal. 2020, 10, 999−1009

pubs.acs.org/acscatalysis

Unraveling the High Activity of Ylide-Functionalized Phosphines in Palladium-Catalyzed Amination Reactions: A Comparative Study with ^{Cy}JohnPhos and P*t*Bu$_3$

Lennart T. Scharf, Ilja Rodstein, Michelle Schmidt, Thorsten Scherpf, and Viktoria H. Gessner*

Chair of Inorganic Chemistry II, Faculty of Chemistry and Biochemistry, Ruhr University Bochum, Universitätsstrasse 150, 44780 Bochum, Germany

Supporting Information

ABSTRACT: Comprehensive mechanistic insights into the activity of different catalysts based on different ligands are important for further ligand design and catalyst improvement. Herein, we report a combined computational and experimental study on the mechanism and catalytic activity of the ylide-substituted phosphine $Cy_3P{-}C(Me)PCy_2$ (keYPhos, **L1**) in C−N coupling reactions including a comparison with the established and often-applied phosphines ^{Cy}JohnPhos (**L2**) and P(*t*Bu)$_3$ (**L3**). Density functional theory (DFT) calculations together with the possible isolation of several intermediates within the catalytic cycle demonstrate that **L1** readily forms low-coordinated palladium complexes [such as **L1·Pd(dba)**], which easily undergo oxidative addition and subsequent amine coordination as well as reductive elimination. Due to the possible opening and closing of the P−C−P angle in **L1**, the steric bulk can be adjusted to the metal environment so that **L1** retains its conformation throughout the whole catalytic cycle, thus leading to fast catalysis at room temperature. Comparative studies of the three ligands with Pd_2dba_3 as a Pd source show that only **L1** efficiently allows for the coupling of aryl chlorides at room temperature. DFT studies suggest that this is mainly due to the reluctance/inability of **L2** and **L3** to form the catalytically active species under these reaction conditions. In contrast, the YPhos ligand readily forms the prereactive complex and undergoes the first oxidative addition reaction. These observations are confirmed by kinetic studies, which indicate a short induction period for the formation of the catalytically active species of **L1**, followed by fast catalysis. This behavior of **L1** is due to its unique electronic and steric properties, which support low activation barriers and fast catalyst generation.

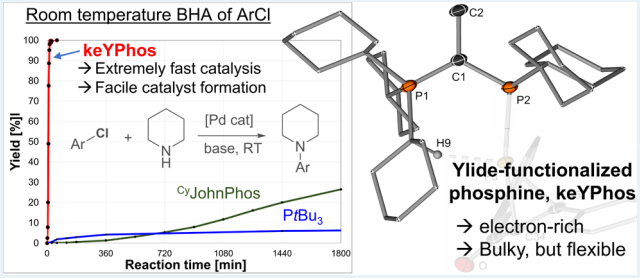

KEYWORDS: *palladium, C−N cross-coupling, phosphines, DFT calculations, reaction mechanism*

INTRODUCTION

The palladium-catalyzed formation of carbon−nitrogen bonds has grown to a mature method in modern organic synthesis for the preparation of complex molecules.[1] Due to the ubiquitous presence of amine functionalities in many agrochemicals, pharmaceuticals, and building blocks in material sciences and other fields of chemistry, it is nowadays used as a valuable tool not only in academia but also in industry. Since the ground-breaking reports by Hartwig and Buchwald in the 1990s,[2] many improvements have been made, often based on the development of new types of ligands and precatalysts. The most important ligand class in Buchwald−Hartwig aminations (BHA) are phosphines. Prominent examples are bidentate phosphines like 2,2′-bis(diphenylphosphino)-1,1′-binaphthyl (BINAP) or 1′-bis(diphenylphosphino)ferrocene (dppf),[3] bulky di- or trialkylphosphines such as Beller's cataCXium A[4] and tris(*tert*-butyl)phosphine[5] as well as Buchwald's biaryl phosphines or the DalPhos ligands by Stradiotto.[6] Particularly, the class of biaryl phosphines has been developed into a library of customized ligands, which master the different demands of different substrates and reaction conditions. This has for example led to the design of ligands that allow reactions under mild conditions or the coupling ofdifficult, such as sterically demanding substrates.[7]

Although many new phosphine ligands are reported each year to further improve the catalytic activity, only a few can compete with the highly elaborated, established ligand systems. However, we recently reported on a new class of phosphine ligands, the ylide-substituted phosphines (YPhos), formed by incorporation of an ylide moiety at the phosphorus center.[8] Without elaborate ligand optimization, these YPhos ligands exhibited unprecedented reactivities in catalysis.[9] In general, YPhos ligands are highly electron-rich phosphines due to the strong electron donation from the ylide substituent to the phosphorus center. This strong donor property is beneficial for the formation of highly efficient catalysts for numerous

Received: October 30, 2019
Revised: December 11, 2019
Published: December 11, 2019

DOI: 10.1021/acscatal.9b04666
ACS Catal. 2020, 10, 999−1009

different transformations. For example, without tedious optimizations of the ligand design, YPhos ligand $^{Cy}Y_{Me}PCy_2$ (keYPhos, **L1**, Figure 1) together with Pd_2dba_3 or $Pd(OAc)_2$

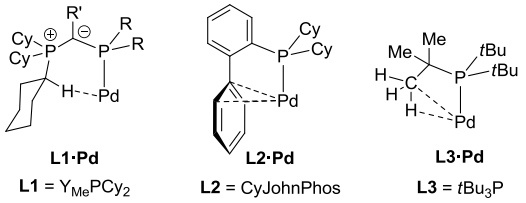

Figure 1. Stabilizing interactions in L·Pd species with **L1**–**L3**.

as metal sources exhibited remarkably high activities in the amination of aryl chlorides at room temperature (RT). Also, difficult, sterically bulky substrates were coupled within mostly a 1 h reaction time.[9]

To further improve the design of the YPhos ligands for palladium catalysis, we became interested in the origin of this remarkable activity. In our initial report, we suggested that the unusual activity of **L1** can be attributed to two factors: (i) the strong donor ability of the ligand [TEP(**L1**) = 2050.1 cm^{-1}][9] and (ii) a weak agostic C–H···Pd interaction in the active Pd(0) species, which stabilizes the Pd(0) complexes and thus facilitates the formation of monoligated Pd species. To gain further insights into the role and behavior of the ligand in the catalytic cycle and to understand the high activity of **L1**, we addressed mechanistic studies of the C–N cross-coupling reaction with **L1**. We were particularly interested in the coordination behavior of **L1** toward palladium in the different complexes formed during catalysis to establish a structure–activity relationship and to facilitate further ligand improvements. Furthermore, a comparative study with established ligands [^{Cy}JohnPhos (**L2**), tBu_3P (**L3**)] was carried out to single out the importance of the different ligand architectures and stabilizing ligand–metal interactions for the different catalytic activities (Figure 1).[9]

RESULTS AND DISCUSSION

Comparative Catalytic Studies. Preliminary studies indicated a considerably higher activity of palladium catalysts based on **L1** after a 1 h reaction time compared to catalysts prepared with ^{Cy}JohnPhos (**L2**) and tBu_3P (**L3**).[9] To further probe the different activities, we carried out more detailed studies on the progress of the reaction. We chose chlorobenzene, *p*-chlorotoluene, and *p*-chlorofluorobenzene as aryl halides together with piperidine as an amine to also probe the impact of different aryl chlorides. All reactions were carried out under the exact same reaction conditions including a preactivation time of 30 min for the catalyst formation from the free ligand and Pd_2dba_3 prior to the addition of the reagents.

As shown in Table 1, the performance of **L1** significantly surpasses that observed for **L2** and **L3**. For all aryl chlorides, full conversion was observed with the YPhos ligand after only a 2 h reaction time. In contrast, only minor amounts of product were formed with **L2** and **L3** even after a 6 h reaction time. This surprisingly strong difference in activity led us to look more closely into the mechanism of the BHA with **L1** and differences compared to **L2** and **L3**.

Structures of Pd(0) Complexes with L1: the Catalytically Active Species. We began our studies with the

Table 1. BHA of Chlorobenzene, *p*-Chlorofluorobenzene, and *p*-Chlorotoluene with Piperidine using Pd_2dba_3 and the Ligands L1–L3[a]

substrate	ligand	0.5 h	1	2	6	24
C_6H_5Cl	**L1**	82	99	100		
	L2	<1	<1	<1	2	20
	L3	<1	2	2	4	6
p-FC_6H_4Cl	**L1**	80	94	100		
	L2	<1	<1	<1	<1	8
	L3	<1	<1	1	2	2
	L1	99	100			
p-MeC_6H_4Cl	**L2**	<1	<1	<1	1	20
	L3	<1	<1	1	2	4

[a]Conditions: 1.5 equiv KO*t*Bu, tetrahydrofuran (THF), 0.5 mol % ligand, 0.25 mol % Pd_2dba_3·dba, RT. The ligand and Pd_2dba_3·dba were stirred for 30 min before addition to the reaction mixture. Conversions were determined by GC with tetradecane as the standard.

elucidation and characterization of catalytically active Pd(0) complexes with **L1**. In our initial publication, we reported on the isolation of the monophosphine complex **L1·Pd(dba)** formed by the addition of $Pd_2(dba)_3$ to a solution of **L1** in THF.[9] This complex exhibited a short C–H···Pd distance, which, together with computational methods, suggested the presence of an agostic interaction (Figure 2). Stability tests

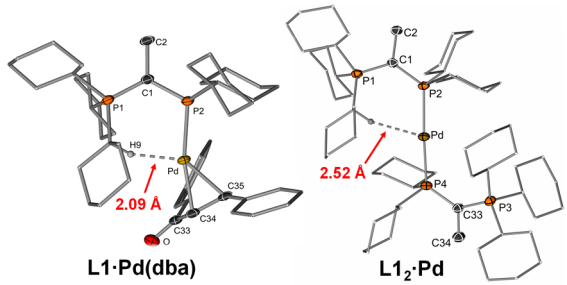

Figure 2. Solid-state structures of Pd(0) complexes with **L1**. Thermal ellipsoids at 50% probability (hydrogen atoms omitted for clarity, except for those binding to Pd). Selected bond lengths (Å) and angles (deg) for **$L1_2$Pd**: Pd–P4 2.3247(6), Pd–P2 2.3382(5), Pd–H3 2.52(3), P1–C1 1.707(2), P2–C1 1.784(2), P3–C33 1.708(3), P4–C33 1.774(3), C3–H3 1.01(3), P4–Pd–P 2165.66(2), P1–C1–P2 125.7(1), P3–C33–P4 127.1(1).

showed that this species slowly decomposes in THF solution, forming Pd black and the free phosphine ligand. The first signs of decomposition were observed in the ^{1}H NMR spectrum within 24 h in THF.

To gain more information about the coordination behavior of **L1** toward Pd(0), the synthesis of a bisphosphine complex was performed. While the reaction of **L1** with $Pd_2(dba)_3$ in a 1:1 metal to ligand ratio selectively led to **L1·Pd(dba)**, the use of 2 equiv of ligand resulted in the formation of the desired bisphosphine complex **$L1_2$·Pd** in THF solution at room temperature. However, no full conversion to **$L1_2$·Pd** was observed under these reaction conditions. Significant amounts (more than 50%) of **L1·Pd(dba)** together with the free phosphine were still present in solution even after a prolonged reaction time [see Figure S1, Supporting Information (SI)]. Fortunately, small amounts of **$L1_2$·Pd** precipitated directly from the reaction mixture as a colorless crystalline solid. Thus,

DOI: 10.1021/acscatal.9b04666
ACS Catal. 2020, 10, 999–1009

the complex could be identified by $^{31}P\{^{1}H\}$ NMR spectroscopy and X-ray crystallography (Figure 2). Alternatively, **L1$_2$·Pd** can also be prepared from (TMEDA)PdMe$_2$ and 2 equiv **L1** (see SI). The bisphosphine complex is stable in the solid state for months, but, similar to the dibenzylideneacetone (dba) complex, exhibits limited stability in solution, which, together with the low solubility, prevented its full characterization. The Pd−P distances in **L1$_2$·Pd** amount to 2.3247(6) and 2.3382(5) Å and are thus comparable to the one found in the dba complex [2.3318(9) Å], but longer compared to other bisphosphine complexes,[10] e.g., 2.265(2) Å in Pd[P(*i*Pr)-(*t*Bu)$_2$]$_2$[11] or 2.285(3) Å in Pd(P*t*Bu$_3$)$_2$.[12] The observed bond elongation is most probably caused by the steric bulk of the ligand and is necessary to allow for the accommodation of both ligands at a single Pd center.

The formation of the bisphosphine complex is rather surprising since the buried volume of the ligand derived from the gold(I) complex **L1·AuCl** was calculated to be 49%, which is larger than the one reported for most of the phosphine ligands in the literature.[13] Thus, the two ligands barely fit around the metal center. The fact that **L1$_2$·Pd** can still be formed at room temperature can be explained by the unique architecture of the YPhos ligand. The ylide moiety in the ligand is more flexible than structures solely based on rigid aryl groups. Particularly, the P−C−P angle varies significantly and thus adjusts to the spatial demand of the metal and its coligands. For example, in the case of **L1$_2$·Pd**, the P−C−P angle amounts to 125.7(1)°, while an angle of 119.1(2)° is observed in the free ligand and 117.4(3)° in **L1·Pd(dba)**. The smaller angle in the dba complex results in a stronger shielding of the metal center by **L1** than in the bisphosphine complex and can be rationalized by the different bulk of dba and **L1**.

As shown in Figure 2, the Pd−H distance to the PCy$_3$ moiety considerably elongates in the bisphosphine complex (2.52(3) Å; Pd−C: 3.490(1) Å) compared to **L1·Pd(dba)** [Pd−H: 2.09(1); Pd−C: 3.010(2) Å], thus suggesting a weakening of the agostic interaction in **L1$_2$·Pd**. Nonetheless, the distance is still in the range of other reported agostic interactions in palladium−phosphine complexes.[14] This is confirmed by computational studies [PBE0-D3/def2svp//def2tzvp + LANL2TZ(f) with THF as a solvent]. Quantum theory of atoms in molecules (QTAIM) calculations yields bond-critical points for the Pd−H interaction for both complexes, whereas the calculated electron density at the bond-critical point (BCP) is considerably higher in the case of the dba complex [q(BCP) = 0.044] than in **L1$_2$·Pd** [q(BCP) = 0.018—two BCPs present]. This is also in line with the natural bond orbital (NBO) analyses and the calculated Wiberg bond indices (see Table S10, SI). The weaker agostic interaction in **L1$_2$·Pd** probably results from steric congestions in the complex. The widening of the P−C−P angle in the ylide substituent (vide supra) ultimately leads to a larger distance between the PCy$_3$ moiety and the metal and thus to a weaker C−H···Pd interaction. Hence, the molecular structures and computational studies demonstrate that the agostic interaction in the YPhos−palladium complexes is strongly sensitive to steric influences. It is noteworthy that there is a Pd−H interaction in **L1$_2$·Pd**, while none is found in Pd(P*t*Bu$_3$)$_2$ (**L3$_2$·Pd**). This is mainly due to the different geometries of the two ligands. In case of the δ-agostic interaction with the YPhos ligand, the hydrogen of the cyclohexyl moiety directly points toward the palladium center. Thus, an almost linear C−H−Pd interaction [159(2)°] is observed in **L1$_2$·Pd**. In contrast, the CH$_3$ protons in **L3$_2$·Pd** point away from the metal [cf. crystal structures with P(*t*Bu)$_{3-n}$R$_n$],[11,12] resulting in a rather bent C−H−Pd interaction (approx. 120° for **L3$_2$·Pd**).

Density functional theory (DFT) calculations [PBE0-D3/def2svp//def2tzvp + LANL2TZ(f), polarizable continuum model (PCM) model with THF as a solvent] show that the bisphosphine complex **L1$_2$·Pd** is thermodynamically more stable than the dba complex **L1·Pd(dba)** ($\Delta\Delta G$ = 38 kJ·mol^{-1}). In the experiment, the formation of the complexes can be controlled by the ligand/metal ratio. Exclusive formation of **L1·Pd(dba)** is found in solution when employing a 1:1 ratio. Since this ratio is used in catalysis,[9] we assume that **L1·Pd(dba)** is the most dominant species for entering the catalytic cycle at the beginning of the catalysis and the formation of the catalytically active species. The fact that a monophosphine species is the active species is further supported by the observation that isolated **L1$_2$·Pd** is catalytically incompetent. No product formation was observed for the coupling of 4-chlorotoluene or 4-fluorochlorobenezene with piperidine under the same reaction conditions as described above (Table 1). This clearly shows that **L1$_2$·Pd** is not an active species and thus not (or only a minor side-product) formed during catalysis. This is further confirmed by the fact that excessive phosphine is needed to quench the activity of **L1** with Pd$_2$dba$_3$. In the coupling of 4-chlorotoluene with piperidine, only a minor loss of activity is observed when using 2 equiv **L1** (Table 2), since C−N coupling is faster than

Table 2. Coupling of *p*-Chlorotoluene with Piperidine Depending on the Amount of L1[a]

entry	**L1** (mol %)	Pd$_2$(dba)$_3$ (mol %)	**L1**/Pd	yield (%)[b]
1	0.5	0.25	1:1	>99
2	1	0.25	2:1	94
3	2	0.25	4:1	79

[a]Reaction conditions: 1 equiv *p*-chlorotoluene, 1.1 equiv piperidine, 1.5 equiv KO*t*Bu, room temperature, 30 min, 0.25 mol % Pd$_2$(dba)$_3$·dba, THF, **L1**. [b]Determined by NMR spectroscopy with trimethoxybenzene as the internal standard.

L1$_2$·Pd formation. With 0.25 mol % of Pd$_2$dba$_3$, full conversion is observed with a 1:1 metal ligand ratio after only a 30 min reaction time, while 94% conversion was achieved with double the amount of ligand. With 4 equiv **L1**, a further drop in activity is found, which suggests the formation of inactive **L1$_2$·Pd** and hence reduction of the catalyst concentration under these conditions. Overall, these data demonstrate that oxidative addition (OA) of the aryl halide occurs at a monoligated palladium complex, which is also in line with kinetic studies by Hartwig and co-workers on bulky trialkylphosphines[15] as well as computational studies such as those by Barder and Buchwald,[16] Norrby,[17] and others.[18]

In Pd-catalyzed coupling reactions, monophosphine species of type R$_3$P·Pd are often supposed to be the catalytically active species. With **L1**, however, the "naked" monoligated complex **L1·Pd** is by far less stable than **L1·Pd(dba)** ($\Delta\Delta G$ = 127 kJ·mol^{-1}) or **L1$_2$·Pd** ($\Delta\Delta G$ = 165 kJ·mol^{-1}), making it unlikely that **L1·Pd** is on the reaction path.[19] Instead, it is more likely that under catalytic conditions, the dba ligand is replaced via an associative mechanism directly by the haloarene to form the prereactive arene complex **1**. Analogous Pd(0)−arene complexes have also been proposed for other phosphine ligands.[20] Based on the calculated energies, it is likely that **L1·**

DOI: 10.1021/acscatal.9b04666
ACS Catal. 2020, 10, 999−1009

Pd(ArCl) (**1**) is the actual active species from which the catalytic cycle starts.[17] The prereactive complex **1** with chlorobenzene as an electrophile is also higher in energy than the dba complex ($\Delta\Delta G$ = 77 kJ·mol^{-1}). However, with the large excess of substrate under catalysis conditions, it should be easily accessible. Applying corrections for the concentrations used in the experiment (0.5 mol % catalyst) decreases the preference of **L1·Pd(dba)** over **1** by 18.8 kJ·mol^{-1} to 59 kJ·mol^{-1}. An analogous energetic difference was also reported for P*t*Bu$_3$·Pd relative to the diphosphine complex.[20] Likewise, the formation of a THF complex, **L1·Pd**·THF, is feasible. This complex is 17 kJ·mol^{-1} (11 kJ·mol^{-1} with concentration correction, respectively) higher in energy than **1** so that this complex is probably formed at the end of catalysis when the substrate concentration is decreasing.

The calculated energies nicely reflect the stability of the dba complex **L1·Pd(dba)** and **L1$_2$·Pd**. However, the high energetic preferences of these species particularly in comparison with the prereactive arene complex **1**, which needs to be formed to enter the catalytic cycle, are somewhat in contradiction to the fast catalysis at room temperature. We believe that this discrepancy is to some extent due to an overestimation of dispersion effects.[21] The inclusion of dispersion effects is crucial for the correct description of large molecular structures like the complexes based on **1**, where, owing to the many cyclohexyl moieties, multiple attractive interactions are present within the molecule. This has often been demonstrated in the literature also for organometallic complexes.[22] However, also, an overestimation of the dispersion interactions has repeatedly been discussed for very large systems.[23] This might also be the case in our complexes, which show considerably high differences between the dispersion-corrected and noncorrected energies (Scheme 1). For example, arene complex **1** is

Scheme 1. Energies at the PBE0(THF)/def2tzvp Level of Theory (with THF as a Solvent) of the Different Pd(0) Species with L1[a]

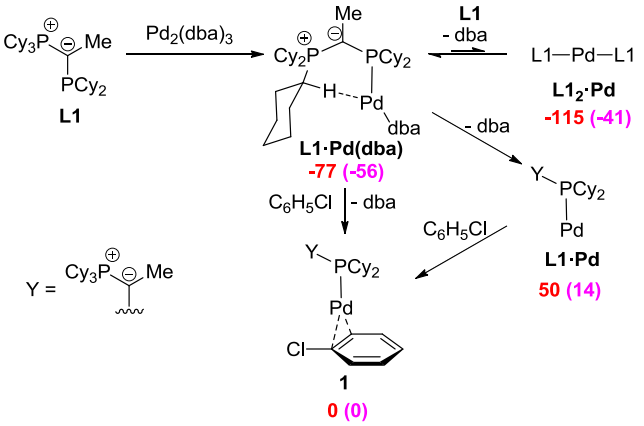

[a]Energies (red = with dispersion effects; purple = without dispersion effects) are given relative to complex **1** in kJ·mol^{-1}.

calculated to be 115 kJ·mol^{-1} higher in energy than the diphosphine complex **L1$_2$·Pd**, while it is disfavored by only 41 kJ·mol^{-1} without the inclusion of dispersion effects. The difference for **L1·Pd** is even larger (165 vs 55 kJ·mol^{-1}). Thus, dispersion effects might result in a somewhat overestimated preference of **L1$_2$·Pd** in comparison to all other structures. This is also indicated by the fact that experimentally, **L1$_2$·Pd** is only observed in the presence of more than 1 equiv of phosphine, while otherwise, only **L1·Pd(dba)** is formed. Consistently, the energy differences between **L1$_2$·Pd** and **1** as well as **L1$_2$·Pd** and **L1·Pd** calculated with the M06 functional, which only considers short- and medium-range dispersion effects,[24] are between the dispersion-corrected and noncorrected PBE0 energies (82 and 115 kJ·mol^{-1}, respectively). Nonetheless, dispersion correction is necessary to better describe the structures of our compounds and thus only these energies are discussed from now onwards. Since all structures shown below are less crowded than **L1$_2$·Pd**, the overestimation should be minimal for these compounds.

Oxidative Addition and Amine Coordination. The prereactive arene complex **1** readily undergoes oxidative addition to form palladium(II) complex *cis*-**2** (Scheme 2).

Scheme 2. Oxidative Addition of Chlorobenzene and Dimethylamine Coordination to 1[a]

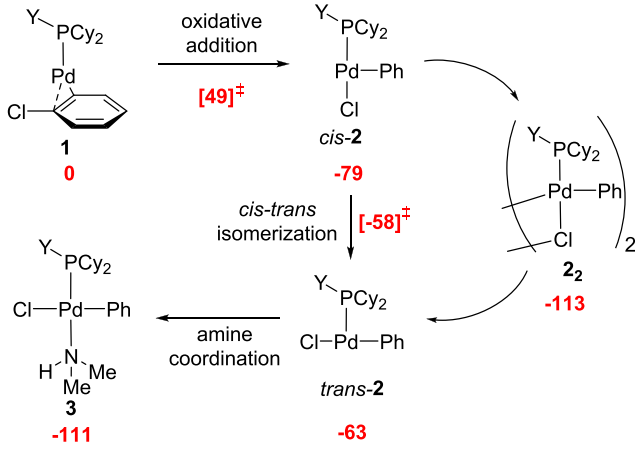

[a]Energies at the PBE0(THF)/def2tzvp level of theory (in kJ·mol^{-1}) are given relative to **1**.

The calculations reveal a low barrier of only 49 kJ·mol^{-1} for the addition of chlorobenzene, which is easily accessible at room temperature and in the range of activation barriers found for aryl chlorides with biaryl phosphines[16] or P(*t*Bu)$_3$.[19b] Also, oxidative addition of aryl chlorides with electron-donating (e.g., −Me or −OMe) and electron-withdrawing substituents (−CN) showed similarly low activation barriers ranging between 47 and 54 kJ·mol^{-1} with **L1** (see Table S18, SI). The structures of the transition state **TS1** and complex *cis*-**2** still feature an agostic interaction with the PCy$_3$ moiety, with Pd−H distances of 2.221 and 2.049 Å. An oxidative addition complex containing two YPhos ligands is not accessible due to steric hindrance.

The oxidative addition product *cis*-**2** is favored over arene complex **1** by 79 kJ·mol^{-1}. Consistently, isolation of the addition product was revealed to be facile also in the experiment. The reaction of a solution of **L1** with Pd$_2$dba$_3$ and an excess of *p*-chlorotoluene in THF at room temperature resulted in the precipitation of **2^{Tol}** (**2^{Tol}** = **2** with *p*-tolyl instead of phenyl) as a yellow solid, which was isolated in a 70% yield and fully characterized. The complex is only poorly soluble in toluene, THF, and other common solvents and decomposes in dichloromethane (DCM) within less than 1 h. In dichloromethane, **2^{Tol}** exhibits two doublets in the ^{31}P{^{1}H} NMR spectrum at 32.5 and 35.1 ppm with a coupling constant of 49.6 Hz. Suitable crystals for X-ray diffraction (XRD)

DOI: 10.1021/acscatal.9b04666
ACS Catal. 2020, 10, 999−1009

analysis were directly obtained from the reaction mixture. $\mathbf{2}^{\mathbf{Tol}}$ crystallizes as a chloro-bridged dimer with a planar $(Cl-Pd)_2$ core (Figure 3). The asymmetric unit contains only half a

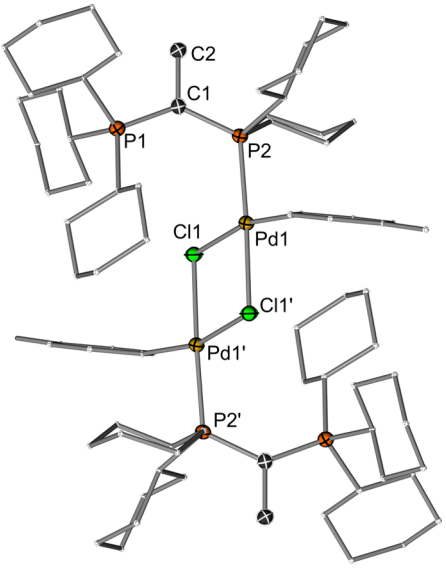

Figure 3. Molecular structure of complex $\mathbf{2_2}^{\mathbf{Tol}}$. Thermal ellipsoids at 50% probability (hydrogen atoms omitted for clarity). Selected bond lengths (Å) and angles (deg): Pd1−C33 1.991(2), Pd1−P2 2.2891(4), Pd1−Cl1 2.4122(4), Pd1−Cl1′ 2.4322(5), P1−C1 1.720(2), P2−C1 1.765(2), C33−Pd1−P2 94.12(5), C33−Pd1−Cl1′ 84.41(5), P2−Pd1−Cl1′ 174.89(2), C33−Pd1−Cl1 164.58(6), P1−C1−P2 131.7(1).

molecule that is assembled through inversion symmetry. Due to the dimeric nature, no C−H···Pd interaction is found. The shortest Pd−H distance in the complex amounts to 2.749(6) Å, which is considerably longer than that in **L1·Pd(dba)**. In accordance with the breaking of the Pd−H interaction, the P1−C1−P2 angle in the oxidative addition product is even larger [131.7(1)°] than that in the bisphosphine complex $\mathbf{L1_2}$**·Pd**, which further confirms the flexibility of the ylide backbone. This widening is necessary to allow for the dimerization. The Pd−P distance is also longer [2.2891(4) Å] compared to other chloro-bridged Pd(II) phosphine complexes.[15,25]

The dimer $\mathbf{2_2}$ is favored by 34 kJ·mol^{-1} over the monomer *cis*-**2**. Although **2** forms a dimer in the solid state, we believe that under the highly diluted catalysis conditions, no dimerization takes place. This has also been reported for other bulky phosphines, which form dimeric oxidative addition products in the solid state and monomers in solution.[15] Unfortunately, attempts to determine the aggregation state in solution by diffusion-ordered spectroscopy (DOSY) NMR experiments failed due to the low solubility of the complex in most solvents or its decomposition such as in DCM. However, further reactivity studies (see below) proved its facile reaction with amines and its catalytic activity, so that independent of its nature in solution, $\mathbf{2_2}$ easily forms the monomeric amine adduct and thus re-enters the catalytic cycle.

The following coordination of the amine (here dimethylamine) to the OA product is diffusion controlled and proceeds smoothly at the trans-isomer of **2**.[26] This trans-isomer is easily accessible by dissociation of the dimer or cis−trans isomerization. The cis and trans forms of T-shaped palladium complexes rapidly equilibrate via a Y-shaped transition state. In the case of **2**, a barrier of 21 kJ·mol^{-1} relative to *cis*-**2** is calculated, so that both forms can readily undergo the next reaction step.[27] The coordination of the amine (Me_2NH) to *trans*-**2** is preferred by 111 kJ·mol^{-1} over **1** and by 30 kJ·mol^{-1} over a possible coordination of the amine to *cis*-**2**. This is due to steric reasons and the trans effect.

Attempts to experimentally obtain structural information about the amine complex were found to be difficult, since in NMR experiments, always mixtures of $\mathbf{2}^{\mathbf{Tol}}$ and $\mathbf{3}^{\mathbf{Tol}}$ were observed, suggesting that both are in equilibrium. Nonetheless, isolation of an amine complex was accomplished with an excess of diethylamine. Treatment of the isolated dimeric oxidative addition complex $\mathbf{2_2}^{\mathbf{Tol}}$ with a large excess of Et_2NH resulted in the formation of complex $\mathbf{3}^{\mathbf{Tol}}$, which could be crystallized by overlayering a THF solution with pentane. $\mathbf{3}^{\mathbf{Tol}}$ is a rare example of an isolated and structurally characterized free amine bound to an oxidative addition complex {LPd(Ar)X} (L = phosphine).[28] The fact that the dimer $\mathbf{2_2}^{\mathbf{Tol}}$ readily forms the amine complex proves its retained catalytic activity and that it is readily cleaved in solution to form a monomeric species. The amine adduct $\mathbf{3}^{\mathbf{Tol}}$ forms a monomeric complex in the solid state (Figure 4) and exhibits agreement with the calculations of

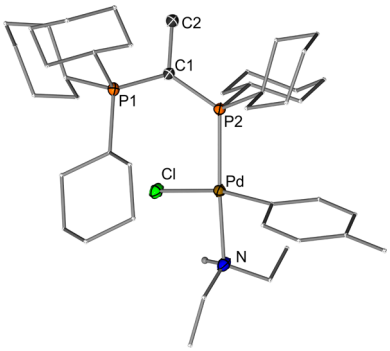

Figure 4. Molecular structure of complex $\mathbf{3}^{\mathbf{Tol}}$. Thermal ellipsoids at 50% probability (hydrogen atoms omitted for clarity). Selected bond lengths (Å) and angles (deg): Pd−C33 2.011(2), Pd−N 2.179(2), Pd−P2 2.3368(5), Pd−Cl 2.4118(5), P1−C1 1.712(2), P2−C1 1.776(2), C33−Pd−N 87.67(8), C33−Pd−P2 94.46(6), N−Pd−P2 172.20(6), C33−Pd−Cl 168.78(6), P1−C1−P2 130.2(1).

the trans-arrangement of the phosphine and the amine. Most interestingly, the PCy_3 moiety of the ligand is still oriented on the same side as the Pd fragment, thus showing that no rotation about the P−C bond is necessary for amine binding. Instead, the P1−C1−P2 angle again widens [130.2(1)°] compared to the less crowded **L1·Pd(dba)** and thus easily allows for the coordination of the amine. The Pd−P distance is again long [2.3368(5) Å]. The chloro and aryl substituent slightly bent away from the YPhos ligand [Cl−Pd−C angle: 168.78(6)°] to avoid steric repulsion.

Reductive Elimination (RE). In the catalytic cycle, the amine complex is next dehydrohalogenated to amido complex **4**, which is the starting point for the following reductive elimination step. The dehydrohalogenation can proceed via different mechanisms, but is usually not considered to be rate determining when using strong metal bases such as metal alkoxides as was used in the case of the YPhos ligand.[27] In the experiment, the amine complex $\mathbf{3}^{\mathbf{Tol}}$ immediately forms the C−N coupling product upon addition of KO*t*Bu as a base, thus preventing the isolation of any intermediate species such as the corresponding amido or amine complex. Calculations confirm

DOI: 10.1021/acscatal.9b04666
ACS Catal. 2020, 10, 999−1009

the fast reaction process. Deprotonation of **3** with *tert*-butoxide as a base ($\Delta G = -30$ kJ·mol^{-1}) and reductive elimination from **4** to amine complex **5** ($\Delta G = -82$ kJ·mol^{-1}) are considerably exergonic. Additionally, reductive elimination possesses only a small activation barrier of $\Delta G^{\ddagger} = 51$ kJ·mol^{-1} for the formation of *N*,*N*-dimethylaniline (Scheme 3). Complex **5** next reacts

Scheme 3. Reductive Elimination from 4 and Reformation of Arene Complex 1[a]

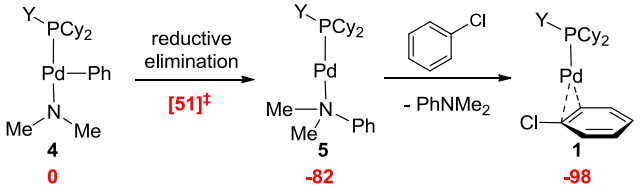

[a]Energies (in kJ·mol^{-1}) at the PBE0(THF)/def2tzvp level are given relative to **1**.

with the aryl chloride to reform the catalytically active arene complex **1** by ligand displacement. Overall, the amido complex **4** is the species with the highest energy in the whole catalytic cycle. Thus, deprotonation by the metal base (e.g., KO*t*Bu) can be viewed as the energy-delivering step from which all further steps are energetically downhill.

We also calculated the energy for the reductive elimination step for a series of other amines. In general, similar energies are observed as for Me_2NH (see Table S18, SI). The highest barriers were found for the primary amines, *tert*-butylamine or 2,6-diisopropylaniline, with barriers of 64 and 67 kJ·mol^{-1}, respectively, which are still sufficiently low to be overcome at room temperature.

Impact of the Ligand Architecture on the Catalyst Activity. Overall, the calculations suggest low activation barriers of approx. 50 kJ·mol^{-1} for the main steps within the catalytic cycle using chlorobenzene and Me_2NH as substrates. This confirms the ease of the C−N coupling reaction with the YPhos ligand at room temperature. Likewise, the formation of the required monoligated palladium species to enter the catalytic cycle seems to be readily accessible from the Pd_2dba_3 precursor. The low barriers and the facile formation of monophosphine complexes are the result of the high donor properties of **L1** in combination with its unique architecture. While agostic interactions between palladium and the PCy_3 moiety stabilize low-coordinate species, this coordination is easily cleaved to open a free coordination site at the metal for substrate (amine) coordination. This opening is realized without any conformational changes within the ligand, which might require substantial activation energy and slow down the process at room temperature. Instead, **L1** retains its conformation in all crystal structures independent of the coordination number and oxidation state of the metal. This is possible because of the flexibility of the ylide backbone, particularly of the P−C−P angle. This angle was found to vary by more than 10°, as can nicely be seen from the superposition of the ligand structures (XRD) in the different complexes (Figure 5). Besides steric protection, small P−C−P angles also provide further electronic stabilization through agostic C−H−Pd interactions by forcing the cyclohexyl groups in proximity to the palladium center. Hence, the reason for the high activity of the keYPhos-based catalyst is, on the one hand, the high donor strength of the ligand and, and on the other hand, its

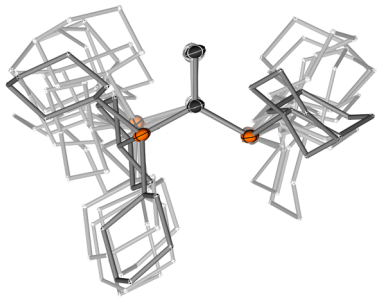

Figure 5. Superposition of the different geometries of **L1** in the different molecular structures of **L1** with and without coordination to a metal.

highly crowded but flexible structure. This concept has also been found to be beneficial for the design of highly active NHC ligands in coupling reactions under mild conditions and thus appears to be a general principle to meet the different requirements in the different steps within a catalytic cycle.[29]

Comparison of L1 with L2 and L3. A comparison of the energies of the important intermediates and transition states for the BHA of phenyl chloride with Me_2NH using the three ligands **L1** (keYPhos), **L2** (^{Cy}JohnPhos), and **L3** ($PtBu_3$) calculated on the same level of theory showed no distinct differences in the activation barriers (Figure 6 and Table 3). All ligands showed similarly low barriers for the oxidative addition or reductive elimination, suggesting that all ligands should undergo fast amination reactions. However, in the experiment, only **L1** gave high yields at room temperature when using $Pd_2(dba)_3$·dba and 1 equiv of ligand as a catalyst (Table 1).[9] Thus, other factors have to be decisive for the observed differences in the activities.

In case of the Buchwald ligands, the required conformational changes within the ligand to open free coordination sites for substrate binding have often been discussed in the literature.[16b,30] In comparison to the biaryl phosphine, the flexibility of **L1** might thus be one reason for its higher activity at room temperature. As shown above, no rotation about the P2−C1 bond is necessary for opening or closing a coordination site at the metal in any step of the catalytic cycle. This is in contrast to the biaryl phosphines, where amine binding is disfavored at the most favored oxidative addition complex (*cis*-**2** with **L2**, Scheme 4). Here, rotation about the P−C bond is necessary to cleave the Pd−arene interaction and allow for a cis−trans isomerization and the binding of the amine trans to the phosphine ligand. This rotation about the P−C bond in the monomeric *cis*-OA complex of **L2** costs approx. 55 kJ·mol^{-1} (Figure 6, top), which sums up to almost 90 kJ·mol^{-1} when considering that the dimeric OA complex is the most favored species prior to this reaction step. Hence, the conformational changes required for amine coordination might become the rate-limiting step for **L2** particularly in case of bulky aryl chlorides. However, for small substrates such as those used in the experiment (Table 1), the calculated barrier should still be sufficiently low for catalysis at room temperature.

Since the barriers within the catalytic cycle seemed to be viable for all ligands, we turned our attention toward the formation of the catalytically active monophosphine complex. The ease of the formation of the L·Pd species has repeatedly been demonstrated to be decisive for the performance of a catalyst. For example, it was shown that the use of $[Pd(PtBu_3)_2]$ as a precatalyst usually requires elevated

DOI: 10.1021/acscatal.9b04666
ACS Catal. 2020, 10, 999−1009

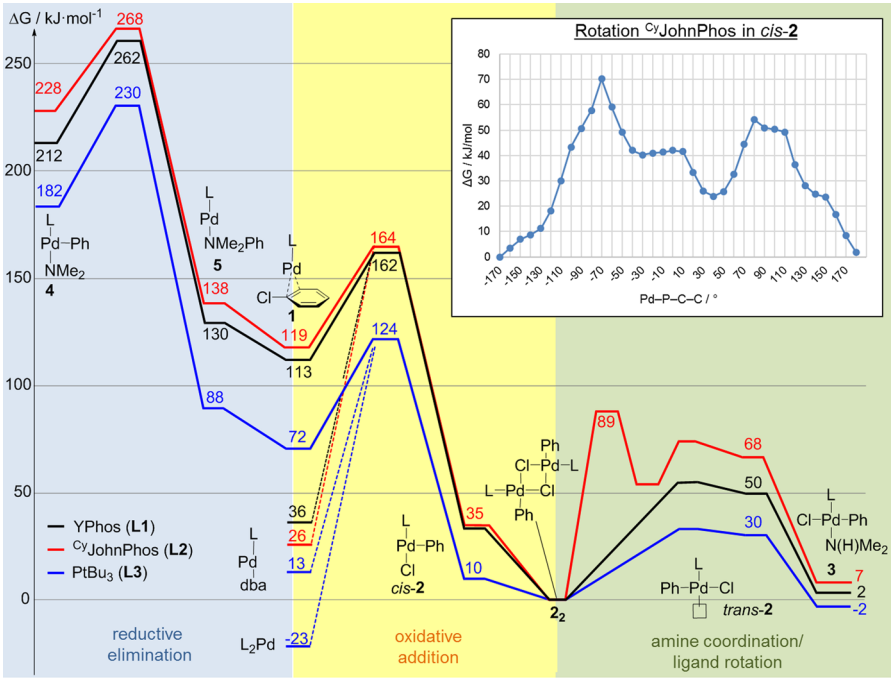

Figure 6. Comparison of the reaction profile [energies at the PBE0-D3(THF)/def2tzvp level] of the amination of chlorobenzene with dimethylamine with **L1**–**L3**.

Table 3. Barriers in kJ·mol^{-1} at the PBE0-D3(THF)/def2tzvp Level for Oxidative Addition (OA) and Reductive Elimination (RE) for L1–L3[a]

ligand	$\Delta G^{\ddagger}$(OA)	$\Delta G^{\ddagger}$(RE)
L1	49	51
L2	46	40
L3	52	48

[a]Energies are given relative to the arene complexes of type **1**.

temperatures for the amination of aryl chlorides,[31] while room-temperature catalysis was described for some combinations with Pd(dba)$_2$ together with 1 equiv of P*t*Bu$_3$.[32] In contrast, the preformed palladium(I) complex [{PdBr(P*t*Bu$_3$)}$_2$], which possess the ideal 1:1 metal ligand ratio, showed similar activities to **L1** at room temperature.[5,33]

A comparison of the energies of the palladium complexes with **L1**–**L3**, which are important for the formation of the catalytically active species, is given in Table 4. For all ligands, the bisphosphine complex L$_2$·Pd is the energetically most favored species. Depending on the functional and dispersion correction, this energetic preference is substantial and implies that the prereactive arene complex L·Pd(PhCl) is hardly formed under the reaction conditions. However, in case of **L1**, and to the best of our knowledge also for **L2**, complex L$_2$·Pd is never formed during catalysis when applying a 1:1 metal ratio (see above). This suggests that there is an appreciable barrier for the formation of L$_2$·Pd for sterically bulky ligands such as **L1** and **L2** [%V_{bur}(**L1**) = 48.5;[9] %V_{bur}(**L2**) = 46.7[13]]. This barrier must be at least as high as the energy of the monoligated complex L·Pd since an associative mechanism starting from L·Pd(dba) is not possible due to steric reasons. In contrast, P*t*Bu$_3$ is considerably smaller [%V_{bur}(**L2**) = 38.1[13]]

Scheme 4. Overview of Rotations for Amine Coordination in YPhos L1 (Black) vs CyJohnPhos L2 (Red)[a]

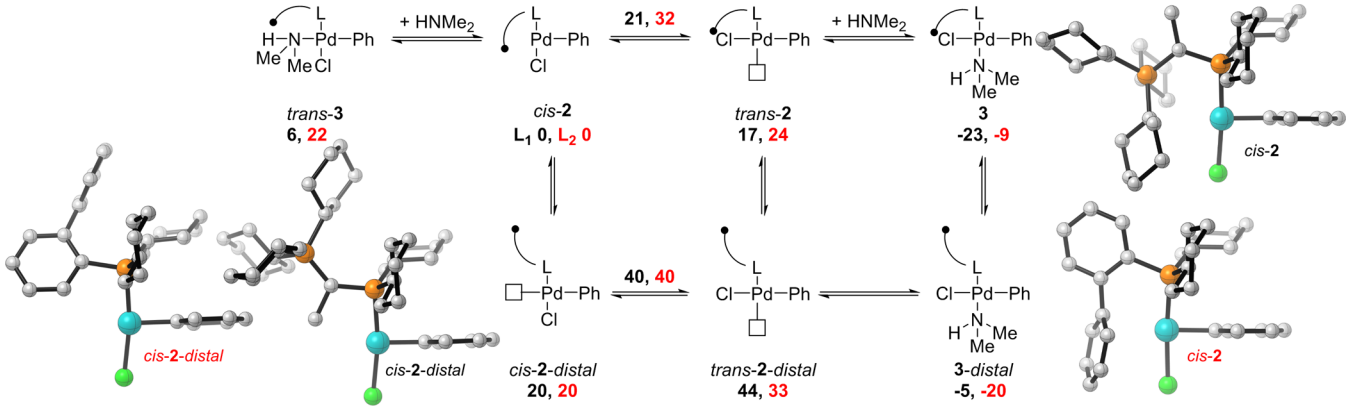

[a]Energies (in kJ·mol^{-1}) are given relative to *cis*-**2**.

DOI: 10.1021/acscatal.9b04666
ACS Catal. 2020, 10, 999–1009

Table 4. Comparison of the Energies of Important Palladium Complexes with L1−L3 as the Starting Point for the Catalysis

ligand	complex	ΔG(PBE0-D3)[a] (kJ·mol^{-1})	ΔG(M06)[b] (kJ·mol^{-1})
keYPhos (**L1**)	L_2·Pd	−115	−82
	L·Pd(dba)	−77	−49
	L·Pd	42	27
	L·Pd(PhCl)	0	0
^{Cy}JohnPhos (**L2**)	L_2·Pd	−98	−79
	L·Pd(dba)	−93	−68
	L·Pd	18	7
	L·Pd(PhCl)	0	0
P*t*Bu$_3$ (**L3**)	L_2·Pd	−95	−87
	L·Pd(dba)	−59	−42
	L·Pd	38	24
	L·Pd(PhCl)	0	0

[a]Energies on the PBE0-D3/def2svp//def2tzvp + LANL2TZ(f) level of theory with THF as a solvent. [b]Energies on the M06/def2tzvp + LANL2TZ(f) level of theory.

and hence L_2·Pd is easily accessible also via an associative mechanism. Once formed, the effective activation barrier for the first oxidative addition of PhCl is higher than 140 kJ·mol^{-1} (Tables 3 and 4) and thus explains the inactivity of P*t*Bu$_3$ at room temperature.[34]

Since **L1** and **L2** do not form L_2·Pd complexes under the reaction conditions, both should enter the cycle from the mixed phosphine−dba complex. Interestingly, L·Pd(dba) is more stable, relative to the prereactive complex L·Pd(PhCl), for **L2** than for **L1**. This means that the first activation energy for the oxidative addition with **L1** is lower [126 (PBE0) or 98 kJ·mol^{-1} (M06)] than that for **L2** [139 (PBE0) or 114 kJ·mol^{-1} (M06)], thus implying that a considerable amount of catalyst with **L2** does not (or very slowly) enter the catalytic cycle at room temperature, which further corroborates with the low conversion observed for the catalysis with **L2**.

Overall, the high activity of keYPhos is not only due to low activation barriers within the cycle but also due to the ease of the formation of the catalytically active species, which is particularly facile for **L1** in comparison to **L2** and **L3**. To experimentally verify the computational results and to probe that the formation of L·Pd(ArCl) is also decisive for **L1**, we turned our attention toward kinetic studies. Reaction monitoring of the amination of 4-chlorotoluene with piperidine using the YPhos ligand showed the presence of a short induction period of approx. 5 min (Figure 7A). We interpret this induction period as the time required for the formation of the active arene complex **L1·Pd**(ArCl) from **L1·Pd(dba)**. Once formed, catalysis is fast and gives full conversion in less than 20 min with 0.5 mol % catalyst loading. The initial reaction rate after the induction period is high and corresponds to a turnover frequency of 1720 h^{-1}, which is a remarkable value for room-temperature BHA of an aryl chloride.

The behavior of **L1** is in stark contrast to the observations made for **L2** and **L3**. As already indicated from the results in Table 1, only little conversion is observed with both ligands after a 6 h reaction time. While this is also true for P*t*Bu$_3$ for a more prolonged reaction time, the reaction with ^{Cy}JohnPhos speeds up after 6 h (Figure 7B) but slows down again after approx. 50 h to finally reach 55% conversion after more than 3 days. The observation for P*t*Bu$_3$ is in line with the hampered formation of the active species and catalyst decomposition. The fact that at least small amounts of product were formed with **L1** can probably be explained by the formation of small amounts of active L·Pd(ArCl) species due to the use of only 1 equiv of ligand.[35] The data obtained for **L2** indicate very slow catalyst formation (6 h) and a rather high activation barrier (low reaction rate) accompanied by catalyst decomposition after a prolonged reaction time. The long induction period is in line with the high energetic difference calculated between L·Pd(dba) and L·Pd(ArCl) with **L2**.

To probe the nature of the rate-limiting step with **L1** as a ligand, we studied the progress of the amination of 4-chlorotoluene with piperidine under different reaction conditions. At first, we used the reaction progress kinetic analysis (RPKA) as described by Blackmond to qualitatively explore the dependence of the reaction rate on the reagent concentrations.[35] To this end, the amination was performed with different [ArCl]/[amine] ratios (different "excess" conditions). As shown in Figure 7C, the reaction rate is not changed by an increase in the amine concentration ([ArCl]/[amine] = 1:2), suggesting that the reaction rate is independent of the amine. In contrast, using 2 equiv of aryl chloride resulted in a marked acceleration of the reaction. The higher reaction rate with higher [ArCl] indicates a positive order in aryl halide. To further examine this dependency in the reagents, we performed a variable time normalization analysis (VTNA) as previously described by Burés.[36] Here, the analysis

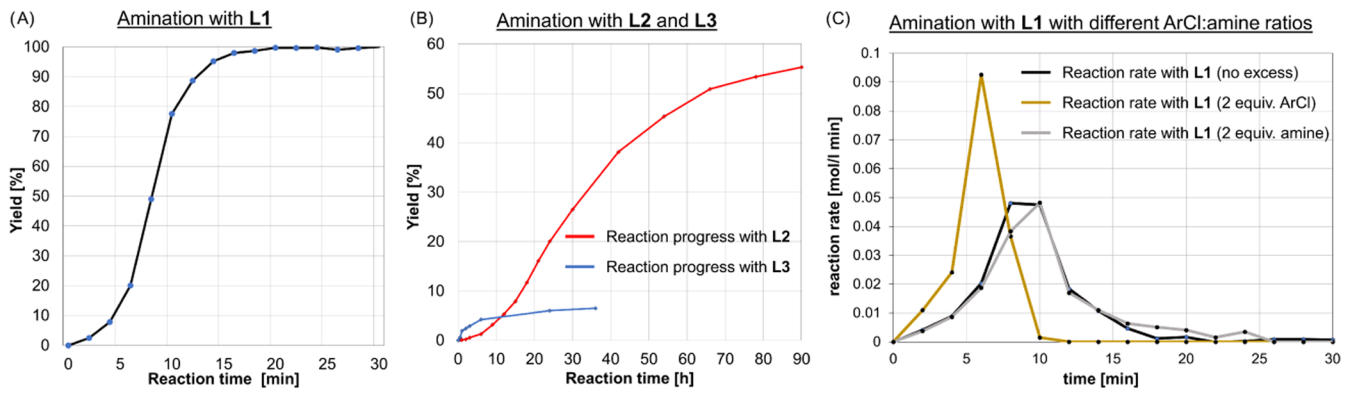

Figure 7. Conversion−time plots for the amination of *p*-chlorotoluene with piperidine with (A) **L1**, (B) with **L2** and **L3**, and (C) plot of the reaction rate under different reaction conditions with **L1**.

DOI: 10.1021/acscatal.9b04666
ACS Catal. 2020, 10, 999−1009

of the obtained data under different reaction conditions is performed by overlaying the different progress concentration profiles (see SI for details). This procedure confirmed the dependence of the reaction rate of the concentration of the aryl chloride and delivered an order of 0.6 in [ArCl]. This observation is well in line with the calculations and the slow formation of LPd(ArCl) from **L1·Pd(dba)**, which makes at least the first oxidative addition step rate limiting. Also, in line with the calculations, the rate was found to be independent of the amine concentration (zeroth order).

Overall, these results demonstrate that the electronic and steric properties of the YPhos ligand both contribute significantly to its high activity. The geometry is particularly important for the facile generation of the active monoligated palladium species, while the donor strength results in low activation barriers. Given the superior performance of defined palladium complexes with phosphine or NHC ligands in catalysis and the fact that the formation of **1** is at least partially contributing to the rate-limiting step, a further improvement of the catalytic ability can also be expected for **L1**.

CONCLUSIONS

The mechanism of the palladium-catalyzed C−N coupling reaction with the YPhos ligand $Cy_3P-C(Me)PCy_2$ (keYPhos, **L1**) was studied by detailed computations and experiments and compared to established phosphines used in this chemistry [JohnPhos (**L2**) and $P(tBu)_3$ (**L3**)]. **L1** readily forms monoligated palladium species, which are stabilized by agostic C−H···Pd interactions and readily undergo oxidative addition reactions with aryl chlorides. Despite the bulk of the ligand, formation of the diphosphine complex **$L1_2$·Pd** as well as dimerization of the oxidative addition complex were found to be possible. This can be explained by the flexibility of the ligand backbone via opening and closing of the P−C−P angle, which allows a certain degree of spatial adjustment depending on the coligands at palladium. Due to this flexibility, no conformational changes are needed along the whole catalytic cycle. This results in low activation barriers for all important steps in the cycle and a minimum of required isomerization processes, which is well in line with the fast catalysis observed at room temperature. While the barriers of the important catalytic steps with **L1** are similar to those found for the biaryl phosphine **L2** and $PtBu_3$ (**L3**), the most pronounced difference between the ligands lies in the formation of the catalytically active arene complex LPd(ArCl). In the case of **L3**, this species is not formed at room temperature due to the high preference of the bisphosphine complex **$L3_2$Pd**. In the case of **L1** and **L2**, the catalytic cycle is entered via the dba complex, which, however, is more stable for **L2**, and thus results in a higher barrier for the first oxidative addition step that is hardly reached at room temperature with **L2**. These computational results are also confirmed by kinetic studies, which also show that the reaction rate for **L1** depends on the aryl chloride and not on the amine.

Overall, these studies demonstrate that the YPhos ligand has ideal characteristics for enabling fast C−N couplings at room temperature. The electronic and steric profile supports low activation barriers and fast catalyst generation. The fact that the aryl chloride is still involved in the rate-limiting step suggests that a further improvement of the catalytic ability also for keYPhos can be expected when using defined precatalysts.

ASSOCIATED CONTENT

Supporting Information

The Supporting Information is available free of charge at https://pubs.acs.org/doi/10.1021/acscatal.9b04666.

Experimental procedures and spectra data for all new and isolated compounds; X-ray crystallographic data for compound **$L1_2$·Pd**, $\mathbf{2_2}^{Tol}$, and $\mathbf{3}^{Tol}$; computational details and coordinates of the energy-optimized structures (PDF)

X-ray crystallographic data file of the OA complex (CIF)

X-ray crystallographic data file of L_2·Pd (CIF)

X-ray crystallographic data file of the amine complex (CIF)

AUTHOR INFORMATION

Corresponding Author

*E-mail: viktoria.gessner@rub.de.

ORCID

Viktoria H. Gessner: 0000-0001-6557-2366

Author Contributions

The manuscript was written through the contributions of all authors. All authors have given approval to the final version of the manuscript.

Funding

This project has received funding from the European Research Council (ERC) under the European Union's Horizon 2020 research and innovation programme (677749).

Notes

The authors declare the following competing financial interest(s): The authors have filed patent WO2019030304 covering the YPhos ligands and precatalysts discussed, which is held by UMICORE and products will be made commercially available from.

ACKNOWLEDGMENTS

We thank the European Research Council (ERC) and the Fonds der Chemischen Industrie (fellowship to L.T.S.) for financial support and Umicore AG & Co. for the supply of palladium complexes.

ABBREVIATIONS

BCP,bond-critical point; BHA,Buchwald−Hartwig aminations; dba,dibenzylideneacetone; **L1**,YPhos ligand $Cy_3P^+-{}^-C(Me)$-PCy_2; **L2**,^{Cy}JohnPhos; OA,oxidative addition; **L3**,$PtBu_3$; RE,reductive elimination; XRD,X-ray diffraction

REFERENCES

(1) (a) Heravi, M. M.; Kheilkordi, Z.; Zadsirjan, V.; Heydari, M.; Malmir, M. Buchwald-Hartwig reaction: An overview. *J. Organomet. Chem.* **2018**, *861*, 17−104. (b) Ruiz-Castillo, P.; Buchwald, S. L. Applications of Palladium-Catalyzed C−N Cross-Coupling Reactions. *Chem. Rev.* **2016**, *116*, 12564−12649. (c) Buchwald, S. L.; Mauger, C.; Mignani, G.; Scholz, U. Industrial-Scale Palladium-Catalyzed Coupling of Aryl Halides and Amines − A Personal Account. *Adv. Synth. Catal.* **2006**, *348*, 23−39. (d) Hazari, N.; Melvin, P. R.; Beromi, M. M. Well-defined nickel and palladium precatalysts for cross-coupling. *Nat. Rev. Chem.* **2017**, *1*, No. 0025. (e) Hartwig, J. F. Discovery and Understanding of Transition-Metal-Catalyzed Aromatic Substitution Reactions. *Synlett* **2006**, 1283−1294.

(2) (a) Paul, F.; Patt, J.; Hartwig, J. F. Palladium-catalyzed formation of carbon-nitrogen bonds. Reaction intermediates and catalyst improvements in the hetero cross-coupling of aryl halides and tin

DOI: 10.1021/acscatal.9b04666
ACS Catal. 2020, 10, 999−1009

amides. *J. Am. Chem. Soc.* **1994**, *116*, 5969−5970. (b) Guram, A. S.; Buchwald, S. L. Palladium-Catalyzed Aromatic Aminations with in situ Generated Aminostannanes. *J. Am. Chem. Soc.* **1994**, *116*, 7901−7902.

(3) (a) Driver, M. S.; Hartwig, J. F. A Second-Generation Catalyst for Aryl Halide Amination: Mixed Secondary Amines from Aryl Halides and Primary Amines Catalyzed by (DPPF)$PdCl_2$. *J. Am. Chem. Soc.* **1996**, *118*, 7217−7218. (b) Wolfe, J. P.; Wagaw, S.; Buchwald, S. L. An Improved Catalyst System for Aromatic Carbon−Nitrogen Bond Formation: The Possible Involvement of Bis(Phosphine) Palladium Complexes as Key Intermediates. *J. Am. Chem. Soc.* **1996**, *118*, 7215−7216. (c) Hartwig, J. F. Evolution of a Fourth Generation Catalyst for the Amination and Thioetherification of Aryl Halides. *Acc. Chem. Res.* **2008**, *41*, 1534−1544. (d) Mann, G.; Hartwig, J. F.; Driver, M. S.; Ferna′ndez-Rivas, C. Palladium-Catalyzed C−N(sp2) Bond Formation: N-Arylation of Aromatic and Unsaturated Nitrogen and the Reductive Elimination Chemistry of Palladium Azolyl and Methyleneamido Complexes. *J. Am. Chem. Soc.* **1998**, *120*, 827−828.

(4) (a) Zapf, A.; Ehrentraut, A.; Beller, M. A New Highly Efficient Catalyst System for the Coupling of Nonactivated and Deactivated Aryl Chlorides with Arylboronic Acids. *Angew. Chem., Int. Ed.* **2000**, *39*, 4153−4155. (b) Köllhofer, A.; Pullmann, T.; Plenio, H. A versatile catalyst for the Sonogashira coupling of aryl chlorides. *Angew. Chem., Int. Ed.* **2003**, *42*, 1056−1058. (c) Ehrentraut, A.; Zapf, A.; Beller, M. Progress in the Palladium-Catalyzed α-Arylation of Ketones with Chloroarenes. *Adv. Synth. Catal.* **2002**, *344*, 209−217.

(5) Stambuli, J. P.; Kuwano, R.; Hartwig, J. F. Unparalleled Rates for the Activation of Aryl Chlorides and Bromides: Coupling with Amines and Boronic Acids in Minutes at Room Temperature. *Angew. Chem., Int. Ed.* **2002**, *41*, 4746−4748.

(6) (a) Lundgren, R. J.; Peters, B. D.; Alsabeh, P. G.; Stradiotto, M. A *P,N*-ligand for palladium-catalyzed ammonia arylation: coupling of deactivated aryl chlorides, chemoselective arylations, and room temperature reactions. *Angew. Chem., Int. Ed.* **2010**, *49*, 4071−4074. (b) Lundgren, R. J.; Stradiotto, M. Palladium-catalyzed cross-coupling of aryl chlorides and tosylates with hydrazine. *Angew. Chem., Int. Ed.* **2010**, *49*, 8686−8690.

(7) (a) Dennis, J. M.; White, N. A.; Liu, R. Y.; Buchwald, S. L. Breaking the Base Barrier: An Electron-Deficient Palladium Catalyst Enables the Use of a Common, Soluble Base in C−N Coupling. *J. Am. Chem. Soc.* **2018**, *140*, 4721−4725. (b) Park, N. H.; Vinogradova, E. V.; Surry, D. S.; Buchwald, S. L. Design of New Ligands for the Palladium-Catalyzed Arylation of α-Branched Secondary Amines. *Angew. Chem., Int. Ed.* **2015**, *54*, 8259−8262. (c) Ruiz-Castillo, P.; Blackmond, D. G.; Buchwald, S. L. Rational Ligand Design for the Arylation of Hindered Primary Amines Guided by Reaction Progress Kinetic Analysis. *J. Am. Chem. Soc.* **2015**, *137*, 3085−3092.

(8) (a) Scherpf, T.; Schwarz, C.; Scharf, L. T.; Zur, J.-A.; Helbig, A.; Gessner, V. H. Ylide-Functionalized Phosphines: Strong Donor Ligands for Homogeneous Catalysis. *Angew. Chem., Int. Ed.* **2018**, *57*, 12859−12864. (b) Scherpf, T.; Wirth, R.; Molitor, S.; Feichtner, K.-S.; Gessner, V. H. Bridging the Gap between Bisylides and Methandiides: Isolation, Reactivity, and Electronic Structure of an Yldiide. *Angew. Chem., Int. Ed.* **2015**, *54*, 8542−8546. (c) Schwarz, C.; Handelmann, J.; Baier, D. M.; Ouissa, A.; Gessner, V. H. Mono- and diylide-substituted phosphines (YPhos): impact of the ligand properties on the catalytic activity in gold(I)-catalysed hydroaminations. *Catal. Sci. Technol.* **2019**, *9*, 6808−6815.

(9) (a) Weber, P.; Scherpf, T.; Rodstein, I.; Lichte, D.; Scharf, L. T.; Gooßen, L. J.; Gessner, V. H. A Highly Active Ylide-Functionalized Phosphine for Palladium-Catalyzed Aminations of Aryl Chlorides. *Angew. Chem., Int. Ed.* **2019**, *58*, 3203−3207. (b) Hu, X.-Q.; Lichte, D.; Rodstein, I.; Weber, P.; Seitz, A.-K.; Scherpf, T.; Gessner, V. H.; Gooßen, L. J. Ylide-Functionalized Phosphine (YPhos)−Palladium Catalysts: Selective Monoarylation of Alkyl Ketones with Aryl Chlorides. *Org. Lett.* **2019**, *21*, 7558−7562.

(10) (a) Reid, S. M.; Boyle, R. C.; Mague, J. T.; Fink, M. J. A Dicoordinate Palladium(0) Complex with an Unusual Intramolecular η^1-Arene Coordination. *J. Am. Chem. Soc.* **2003**, *125*, 7816−7817. (b) Scheuermann, M. L.; Boyce, D. W.; Grice, K. A.; Kaminsky, W.; Stoll, S.; Tolman, W. B.; Swang, O.; Goldberg, K. I. Oxygen-promoted C-H bond activation at palladium. *Angew. Chem., Int. Ed.* **2014**, *53*, 6492−6495. (c) Otsuka, S.; Yoshida, T.; Matsumoto, M.; Nakatsu, K. Bis(tertiary phosphine)palladium(0) and -platinum(0) complexes: preparations and crystal and molecular structures. *J. Am. Chem. Soc.* **1976**, *98*, 5850−5858. (d) Paul, F.; Patt, J.; Hartwig, J. F. Structural Characterization and Simple Synthesis of $\{Pd[P(o\text{-}Tol)_3]_2\}$. Spectroscopic Study and Structural Characterization of the Dimeric Palladium(II) Complexes Obtained by Oxidative Addition of Aryl Bromides and Their Reactivity with Amines. *Organometallics* **1995**, *14*, 3030−3039. (e) Barrett, B. J.; Iluc, V. M. An Adaptable Chelating Diphosphine Ligand for the Stabilization of Palladium and Platinum Carbenes. *Organometallics* **2017**, *36*, 730−741. (f) Lee, S. Y.; Hartwig, J. F. Palladium-Catalyzed, Site-Selective Direct Allylation of Aryl C−H Bonds by Silver-Mediated C−H Activation: A Synthetic and Mechanistic Investigation. *J. Am. Chem. Soc.* **2016**, *138*, 15278−15284. (g) Immirzi, A.; Musco, A. Two-co-ordinate Phosphine-Palladium(0) Complexes: X-Ray Structure of the Tricyclohexyl- and the Di(t-butyl)phenyLphosphine Derivatives. *J. Chem. Soc., Chem. Commun.* **1974**, 400−401. (h) Hill, L. L.; Crowell, J. L.; Tutwiler, S. L.; Massie, N. L.; Hines, C. C.; Griffin, S. T.; Rogers, R. D.; Shaughnessy, K. H.; Grasa, G. A.; Johansson Seechurn, C. C. C.; Li, H.; Colacot, T. J.; Chou, J.; Woltermann, C. J. Synthesis and X-ray Structure Determination of Highly Active Pd(II), Pd(I), and Pd(0) Complexes of Di(*tert*-butyl)neopentylphosphine (DTBNpP) in the Arylation of Amines and Ketones. *J. Org. Chem.* **2010**, *75*, 6477−6488. (i) Sergeev, A. G.; Zapf, A.; Spannenberg, A.; Beller, M. Synthesis and Crystal Structure of Palladium(0) and Arylpalladium-(II) Bromide Complexes of CataCXium A. *Organometallics* **2008**, *27*, 297−300.

(11) Proutiere, F.; Lyngvi, E.; Aufiero, M.; Sanhueza, I. A.; Schoenebeck, F. Combining the Reactivity Properties of PCy_3 and $PtBu_3$ into a Single Ligand, $P(iPr)(tBu)_2$. Reaction via Mono- or Bisphosphine Palladium(0) Centers and Palladium(I) Dimer Formation. *Organometallics* **2014**, *33*, 6879−6884.

(12) Tanaka, M. Structure of bis(tri-*tert*-butylphosphine)palladium-(0). *Acta Crystallogr., Sect. C: Cryst. Struct. Commun.* **1992**, *48*, 739−740.

(13) Clavier, H.; Nolan, S. P. Percent buried volume for phosphine and *N*-heterocyclic carbene ligands: steric properties in organometallic chemistry. *Chem. Commun.* **2010**, *46*, 841−861.

(14) (a) McMullin, C. L.; Rühle, B.; Besora, M.; Orpen, A. G.; Harvey, J. N.; Fey, N. Computational study of PtBu3 as ligand in the palladium-catalysed amination of phenylbromide with morpholine. *J. Mol. Catal. A* **2010**, *324*, 48. (b) Stambuli, J. P.; Incarvito, C. D.; Buehl, M.; Hartwig, J. F. Synthesis, Structure, Theoretical Studies, and Ligand Exchange Reactions of Monomeric, T-Shaped Arylpalladium-(II) Halide Complexes with an Additional, Weak Agostic Interaction. *J. Am. Chem. Soc.* **2004**, *126*, 1184−1194.

(15) Barrios-Landeros, F.; Carrow, B. P.; Hartwig, J. F. Effect of Ligand Steric Properties and Halide Identity on the Mechanism for Oxidative Addition of Haloarenes to Trialkylphosphine Pd(0) Complexes. *J. Am. Chem. Soc.* **2009**, *131*, 8141−8154.

(16) (a) Zhao, Y.; Truhlar, D. G. Benchmark Energetic Data in a Model System for Grubbs II Metathesis Catalysis and Their Use for the Development, Assessment, and Validation of Electronic Structure Methods. *J. Chem. Theory Comput.* **2009**, *5*, 324−333. (b) Barder, T. E.; Buchwald, S. L. Insights into Amine Binding to Biaryl Phosphine Palladium Oxidative Addition Complexes and Reductive Elimination from Biaryl Phosphine Arylpalladium Amido Complexes via Density Functional Theory. *J. Am. Chem. Soc.* **2007**, *129*, 12003−12010.

(17) Ahlquist, M.; Norrby, P.-O. Oxidative Addition of Aryl Chlorides to Monoligated Palladium(0): A DFT-SCRF Study. *Organometallics* **2007**, *26*, 550−553.

(18) (a) Ariafard, A.; Yates, B. F. Subtle Balance of Ligand Steric Effects in Stille Transmetalation. *J. Am. Chem. Soc.* **2009**, *131*, 13981−13991. (b) Lam, K. C.; Marder, T. B.; Lin, Z. DFT Studies on the

DOI: 10.1021/acscatal.9b04666
ACS Catal. 2020, 10, 999−1009

Effect of the Nature of the Aryl Halide Y−C_6H_4−X on the Mechanism of Its Oxidative Addition to Pd^0L versus Pd^0L_2. *Organometallics* **2007**, *26*, 758.
(19) (a) Ahlquist, M. S. G.; Norrby, P.-O. Dispersion and Back-Donation Gives Tetracoordinate $[Pd(PPh_3)_4]$. *Angew. Chem., Int. Ed.* **2011**, *50*, 11794−11797. (b) Lyngvi, E.; Sanhueza, I. A.; Schoenebeck, F. Dispersion Makes the Difference: Bisligated Transition States Found for the Oxidative Addition of $Pd(PtBu_3)_2$ to Ar-OSO_2R and Dispersion-Controlled Chemoselectivity in Reactions with $Pd[P(iPr)(tBu_2)]_2$. *Organometallics* **2015**, *34*, 805−812.
(20) McMullin, C. L.; Jover, J.; Harvey, J. N.; Fey, N. Accurate Modelling of Pd(0) + PhX Oxidative Addition Kinetics. *Dalton Trans.* **2010**, *39*, 10833−10836.
(21) Note that no significant changes in the energies are observed when using different solvent models (PCM or COSMO).
(22) (a) Hansen, A.; Bannwarth, C.; Grimme, S.; Petrović, P.; Werlé, C.; Djukic, J.-P. The Thermochemistry of London Dispersion-Driven Transition Metal Reactions: Getting the 'Right Answer for the Right Reason. *ChemistryOpen* **2014**, *3*, 177−189. (b) Schwabe, T.; Grimme, S.; Djukic, J.-P. Noncovalent Metal-Metal Interactions: The Crucial Role of London Dispersion in a Bimetallic Indenyl System. *J. Am. Chem. Soc.* **2009**, *131*, 14156−14157. (c) Sieffert, N.; Bühl, M. Noncovalent Interactions in a Transition-Metal Triphenylphosphine Complex: A Density Functional Case Study. *Inorg. Chem.* **2009**, *48*, 4622−4624. (d) Grimme, S. Comment on: "On the Accuracy of DFT Methods in Reproducing Ligand Substitution Energies for Transition Metal Complexes in Solution: The Role of Dispersive Interactions" by H. Jacobsen and L. Cavallo. *ChemPhysChem* **2012**, *13*, 1407−1409. (e) Steinmetz, M.; Grimme, S. Benchmark Study of the Performance of Density Functional Theory for Bond Activations with (Ni,Pd)-Based Transition-Metal Catalysts. *ChemistryOpen* **2013**, *2*, 115−124.
(23) (a) Jacobsen, H.; Cavallo, L. On the Accuracy of DFT Methods in Reproducing Ligand Substitution Energies for Transition Metal Complexes in Solution: The Role of Dispersive Interactions. *ChemPhysChem* **2012**, *13*, 562−569. (b) Fey, N.; Ridgway, B. M.; Jover, J.; McMullin, C. L.; Harvey, J. N. Organometallic Reactivity: The Role of Metal−ligand Bond Energies from a Computational Perspective. *Dalton Trans.* **2011**, *40*, 11184−11191.
(24) Zhao, Y.; Truhlar, D. G. Benchmark Energetic Data in a Model System for Grubbs II Metathesis Catalysis and Their Use for the Development, Assessment, and Validation of Electronic Structure Methods. *J. Chem. Theory Comput.* **2009**, *5*, 324−333.
(25) (a) Chaudhari, K. R.; Wadawale, A. P.; Jain, V. K. Isolation of Chloro-Bridged Arylpalladium Complexes, $[Pd_2Ar_2(\mu\text{-}Cl)_2(PR_3)_2]$, in Palladium Catalyzed C−C Cross Coupling Reaction of Triarylbismuth with Arylhalides. *J. Organomet. Chem.* **2012**, *698*, 15−21. (b) Chaudhari, K. R.; Wadawale, A. P.; Kumar, M.; Jain, V. K. Pyrazolato-Bridged Arylpalladium(II) Complexes, $[Pd_2Ar_2(\mu\text{-}Pz/Dmpz)_2(PR_3)_2]$: Synthesis and Characterization. *J. Organomet. Chem.* **2014**, *760*, 55−59.
(26) Sunesson, Y.; Limé, E.; Nilsson Lill, S. O.; Meadows, R. E.; Norrby, P.-O. Role of the Base in Buchwald−Hartwig Amination. *J. Org. Chem.* **2014**, *79*, 11961−11969.
(27) (a) Bäcktorp, C.; Norrby, P.-O. A DFT comparison of the neutral and cationic Heck pathways. *Dalton Trans.* **2011**, *40*, 11308−11314.
(28) (a) Biscoe, M. R.; Barder, T. E.; Buchwald, S. L. Electronic Effects on the Selectivity of Pd-Catalyzed C-N Bond-Forming Reactions Using Biarylphosphine Ligands: The Competitive Roles of Amine Binding and Acidity. *Angew. Chem., Int. Ed.* **2007**, *46*, 7232. (b) Paul, F.; Patt, J.; Hartwig, J. F. Structural Characterization and Simple Synthesis of $\{Pd[P(o\text{-}Tol)_3]_2\}$. Spectroscopic Study and Structural Characterization of the Dimeric Palladium(II) Complexes Obtained by Oxidative Addition of Aryl Bromides and Their Reactivity with Amines. *Organometallics* **1995**, *14*, 3030−3039.
(29) (a) Pompeo, M.; Farmer, J. L.; Froese, R. D. J.; Organ, M. J. Room-Temperature Amination of Deactivated Aniline and Aryl Halide Partners with Carbonate Base Using a Pd-PEPPSI-IPentCl-o-Picoline Catalyst. *Angew. Chem., Int. Ed.* **2014**, *53*, 3223−3226. (b) Zhang, Y.; Lavigne, G.; Lugan, N.; César, V. Buttressing Effect as a Key Design Principle towards Highly Efficient Palladium/ N-Heterocyclic Carbene Buchwald−Hartwig Amination Catalysts. *Chem. − Eur. J.* **2017**, *23*, 13792−13801. (c) Froese, R. D. J.; Lombardi, C.; Pompeo, M.; Rucker, R. P.; Organ, M. J. Designing Pd−N-Heterocyclic Carbene Complexes for High Reactivity and Selectivity for Cross-Coupling Applications. *Acc. Chem. Res.* **2017**, *50*, 2244−2253.
(30) Barder, T. E.; Biscoe, M. R.; Buchwald, S. L. Structural Insights into Active Catalyst Structures and Oxidative Addition to (Biaryl)-phosphine-Palladium Complexes via Density Functional Theory and Experimental Studies. *Organometallics* **2007**, *26*, 2183−2192.
(31) Kuwano, R.; Utsunomiya, M.; Hartwig, J. F. Aqueous Hydroxide as a Base for Palladium-Catalyzed Amination of Aryl Chlorides and Bromides. *J. Org. Chem.* **2002**, *67*, 6479−6486.
(32) Hartwig, J. F.; Kawatsura, M.; Hauck, S. I.; Shaughnessy, K. H.; Alcazar-Roman, L. M. Room-Temperature Palladium-Catalyzed Amination of Aryl Bromides and Chlorides and Extended Scope of Aromatic C-N Bond Formation with a Commercial Ligand. *J. Org. Chem.* **1999**, *64*, 5575−5580.
(33) (a) Keaveney, S. T.; Kundu, G.; Schoenebeck, F. Modular Functionalization of Arenes in a Triply Selective Sequence: Rapid Csp^2 and Csp^3 Coupling of C-Br, C-OTf and C-Cl enabled by a Single Pd(I) Dimer. *Angew. Chem., Int. Ed.* **2018**, *57*, 12573−12577. (b) Sperger, T.; Schoenebeck, F. α-Arylation of Esters and Ketones Enabled by a Bench-Stable Pd(I) Dimer Catalyst. *Synthesis* **2018**, *50*, 4471−4475. (c) Kalvet, I.; Sperger, T.; Scattolin, T.; Magnin, G.; Schoenebeck, F. Palladium(I) Dimer Enabled Extremely Rapid and Chemoselective Alkylation of Aryl Bromides over Triflates and Chlorides in Air. *Angew. Chem., Int. Ed.* **2017**, *56*, 7078−7082. (d) Johansson Seechurn, C. C. C.; Sperger, T.; Scrase, T. G.; Schoenebeck, F.; Colacot, T. J. Understanding the Unusual Reduction Mechanism of Pd(II) to Pd(I): Uncovery of Hidden Species and Implications in Catalytic Cross-Coupling Reactions. *J. Am. Chem. Soc.* **2017**, *139*, 5194−5200.
(34) We would also like to point out that the low-coordinate $PtBu_3$ palladium complexes are presumably less stable towards Pd black formation than those of **L1** and **L2** due to missing/weaker secondary ligand metal interactions.
(35) (a) Blackmond, D. G. Reaction progress kinetic analysis: a powerful methodology for mechanistic studies of complex catalytic reactions. *Angew. Chem., Int. Ed.* **2005**, *44*, 4302−4320. (b) Mathew, J. S.; Klussmann, M.; Iwamura, H.; Valera, F.; Futran, A.; Emanuelsson, E. A. C.; Blackmond, D. G. Investigations of Pd-Catalyzed ArX Coupling Reactions Informed by Reaction Progress Kinetic Analysis. *J. Org. Chem.* **2006**, *71*, 4711−4722.
(36) Nielsen, C. D.-T.; Burés, J. Visual kinetic analysis. *Chem. Sci.* **2019**, *10*, 348−353.

DOI: 10.1021/acscatal.9b04666
ACS Catal. 2020, 10, 999−1009